Available online at www.sciencedirect.com
ScienceDirect
International Journal of Thermal Sciences 46 (2007) 76–92
International Journal of Thermal Sciences
www.elsevier.com/locate/ijts

Combination technique for improving natural convection cooling in electronics

L.A. Florio *, A. Harnoy

Department of Mechanical Engineering, New Jersey Institute of Technology, University Heights, Newark, NJ 07102, USA

Received 30 September 2005; accepted 29 March 2006

Available online 5 June 2006

Abstract

The combination of an appropriately placed cross-flow opening and a strategically positioned transversely vibrating plate is proposed as a means of augmenting pure natural convection in a vertical channel. This method is intended to provide a more efficient, reliable, and consumer conscious alternative to conventional techniques for lower power dissipating devices where standard natural convection cooling proves insufficient. Two-dimensional numerical simulations are employed to investigate this combination method using models consisting of a vertical channel containing two rectangular heat sources which are attached to a vertical mounting board, as well as a transversely oscillating plate and a cross-flow opening in the mounting board area between the two heat sources. Varied parameters and geometric configurations are studied. The results indicate the combined effects of the vibrating plate and the opening flow have the potential to cause significant improvement in the thermal conditions over pure natural convection. As much as a 70% improvement in the local heat transfer coefficient from that for a system with a board opening but without a vibrating plate was attained.

Keywords: Heat transfer enhancement; Natural convection; Oscillations; Numerical modeling

1. Introduction

Natural convection holds obvious advantages for cooling low power dissipating devices due to its low-cost, energy-free, and noise-free operation [1–3]. However, not all systems can be amply cooled by natural convection. A common conventional solution when natural convection is insufficient is to employ a rotating fan. Despite its relatively low cost, the use of a rotating fan is not energy efficient or reliable, creates noise, and requires significant space [1,2,4–9]. The marked contrast between these characteristics and those of pure natural convection provides motivation for the study of unconventional cooling methods that can sufficiently augment natural convection in a manner that preserves its sought after qualities.

In this work, the simultaneous use of an appropriately situated cross-flow opening and a strategically positioned transversely vibrating plate as in Fig. 1(a) is studied as a possible intermediary alternative cooling technique that can locally enhance the natural convection heat transfer from discrete heat sources and reduce the reliance on more conventional, less efficient methods. This combination technique has practical merit as its implementation can lead to quiet, efficient, and compact cooling with the transverse oscillations produced by a device like a vibrating piezoelectric fan and the cross-flow openings generated simply by modifying the mounting board geometry [10–15]. Such traits together with the localized nature of the resulting cooling make this method of particular interest in electronics applications.

A detailed review of the related literature is provided in [19]. The literature reveals not only the limitations in the cooling levels attainable through the independent use of a cross-flow opening or the vibrating plate but also the lack of knowledge about the combined implementation of these methods, particularly with natural convection [7,10–22]. Studies by Florio [19] demonstrate that the cooling effect caused by cross-flow passages placed in the mounting board in the area between the heat sources in a natural convection cooled vertical channel can result in up to a 180% increase in the heat transfer coefficient.

* Corresponding author. Tel.: +1 973 596 3324; fax: +1 973 642 4282.
E-mail address: laf9011@njit.edu (L.A. Florio).

1290-0729/$ – see front matter
doi:10.1016/j.ijthermalsci.2006.03.007

Nomenclature

A	amplitude of oscillation, Eq. (1)	m
b	BH (reference length)	m
BH	heat source height, Fig. 1(b)	m
BL	heat source width, Fig. 1(b)	m
BT	board thickness, Fig. 1(b)	m
$C(t)$	instantaneous clearance, Fig. 1(b), Eq. (1)	m
CHL	lower channel height, Fig. 1(b)	m
CHU	upper channel height, Fig. 1(b)	m
CM	mean clearance, Eq. (1)	m
d	nomenclature Eq. (10)	m
$d_{os}(t)$	instantaneous displacement of oscillating plate Eq. (1)	m
c_p	specific heat	$\mathrm{J\,kg^{-1}\,K^{-1}}$
g	gravitational acceleration	$\mathrm{m\,sec^{-2}}$
Gr	Grashof number, $Gr = \beta g \Delta T_{ref} L_{ref}^3 / v^2$	
h	heat transfer coefficient Eq. (15)	$\mathrm{W\,m^{-2}\,K^{-1}}$
HW	opening width Fig. 1(b)	m
k	thermal conductivity	$\mathrm{W\,m^{-1}\,K^{-1}}$
L	reference x dimension	m
n	normal direction	
PL	length of oscillating plate Fig. 1(b)	m
PT	thickness of oscillating plate Fig. 1(b)	m
P_D	dynamic pressure	Pa
Pr	Prandtl number, $Pr = v/(k/\rho c_p)$	
Q''', Q_a'''	heat rate, applied heat rate	$\mathrm{W\,m^{-3}}$
q	heat flux Eq. (14)	$\mathrm{W\,m^{-2}}$
S2	dimension Fig. 1(b)	m
SL	dimension Fig. 1(b)	m
SPACE	dimension Fig. 1(b)	m
t	time	sec
T	temperature	K
TL	total channel length, Fig. 1(b)	m
u, v	x, y components of velocity	$\mathrm{m\,sec^{-1}}$
$\vec{V}$	velocity vector	$\mathrm{m\,sec^{-1}}$
x, y	coordinates	m

Greek symbols

β	coefficient of thermal expansion	$\mathrm{K^{-1}}$
μ	absolute viscosity	$\mathrm{N\,sec\,m^{-2}}$
v	kinematic viscosity	$\mathrm{m^2\,sec^{-1}}$
ω	oscillation frequency, Eq. (1)	$\mathrm{rad\,sec^{-1}}$
ω	nomenclature, Eq. (10)	
ρ	density	$\mathrm{kg\,m^{-3}}$
ψ	nodal solution values	

Notations

$\widetilde{(\,)}_F$	dimensionless
$\overline{(\,)}$	time average
$\vec{(\,)}$	vector
∇	del operator
$\| \, \|$	sum of root mean square norm

Subscripts

1	related heat source solid
2	related to board/oscillating plate solids
comp	component x, y
o	related to ambient conditions
os	related to oscillating plate
ref	reference for non-dimensionalization

However, the amount of improvement is dependent on the system geometry, particularly the geometry near the opening. The transverse oscillations of a discrete plate placed just atop a discrete heat source can improve the local heat transfer coefficient by 52% and the surface average by 43% [19]. However, the cooling effect appears to approach an upper bound [19,20]. The tandem use of two methods as described is expected to overcome the enhancement limitations that develop when each of these cooling methods is applied separately. In this way, the combination method can help to meet the growing cooling demands and to enable the use of more efficient and effective alternative cooling methods over a broader spectrum of operating conditions and applications.

Therefore, the objective of this work is to use numerical modeling of the two-dimensional systems shown in Fig. 1(a) to investigate the viability of this combination technique to augment natural convection in a vertical channel.

2. Problem investigated

The simplified two-dimensional model shown in Fig. 1(a) is the basis of the parametric finite element studies conducted in this investigation. The system consists of a two heat source array, which could simulate electronic components, attached to a mounting board that is bounded by two parallel vertical channel walls. A cross-flow board opening is placed between the two heat sources and a transversely vibrating plate is introduced to the system with a number of different configurations considered. For compact presentation, each of the four plate locations investigated is shown superimposed in Fig. 1(a) (labeled cases C, D, E, F). A given transient simulation involves only one vibrating plate. In the discussion that follows, the heat source to the left is referred to as heat source 1, while the source on the right is referred to as heat source 2.

In this two-dimensional study, the oscillating plate is rigid and moves in the transverse direction, perpendicular to the plane of the channel walls and the top surfaces of the heat sources. For all system configurations, the instantaneous clearance, $C(t)$, below the moving plate is:

$$C(t) = \mathrm{CM} + d_{os}(t) \quad \text{where } d_{os}(t) = A\sin(\omega t) \tag{1}$$

where CM is the mean clearance spacing, $d_{os}(t)$ is the instantaneous displacement of the vibrating plate from its mean location, A is the oscillation displacement amplitude, and ω is

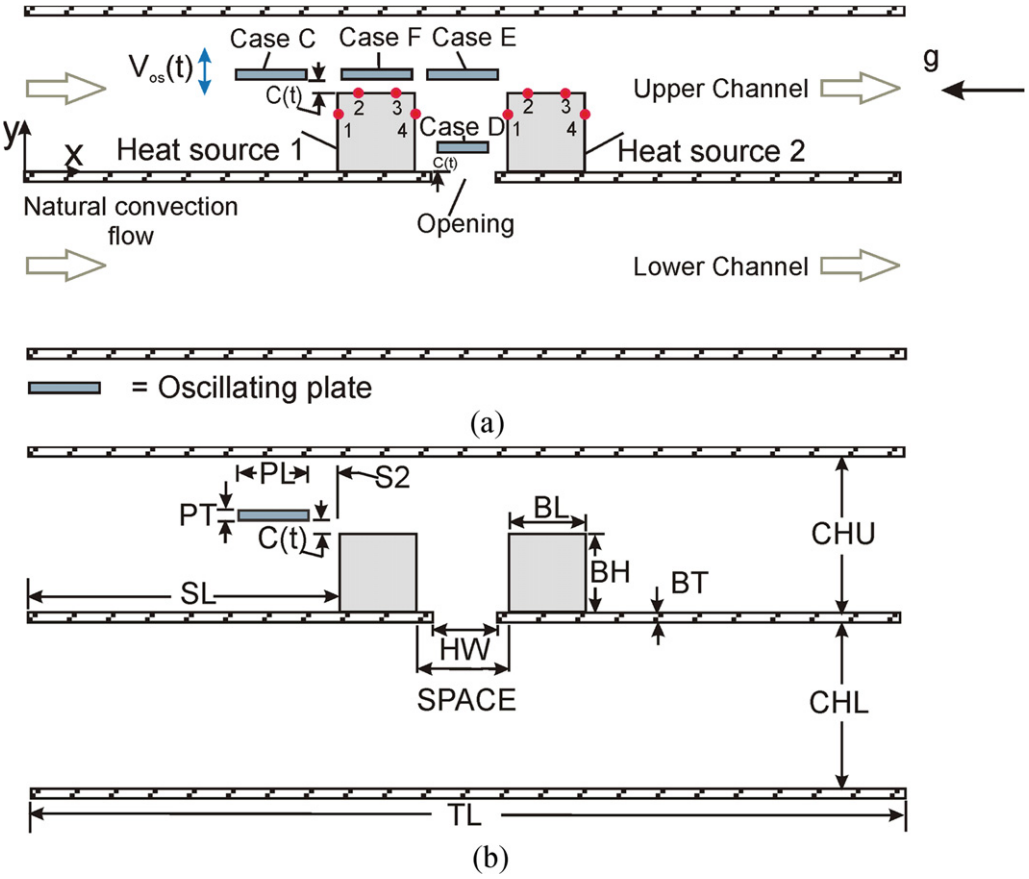

Fig. 1. (a) Four oscillating plate locations investigated denoted by case C, case D, case E, and case F, to examine heat transfer enhancement effects of a single oscillating plate, the cross-flow opening, and natural convection; (b) dimensioning for case C arrangement.

the oscillation frequency. For reference, the dimensioning of the model for the case C arrangement is given in Fig. 1(b). The dimensions for the remaining cases follow similarly, but with the plate centered above either a heat source or the opening as appropriate.

To facilitate a focus on the impact of the plate oscillations for a number of operating conditions for each of the system configurations, the parametric studies performed hold the heat source heat rate and the dimensions of the vibrating plate, heat sources, and channel fixed and vary the displacement amplitudes or frequencies, or for some cases, the mean clearance spacing. The system parameters are provided in Table 1 with the oscillation and clearance parameters listed in Table 3.

For each parameter set and configuration, the numerical simulations are continued until transient, periodically repeating solutions for the velocity and temperature fields have been attained (see Section 2.4). These solutions are referred to as "periodic" solutions in the remainder of this work.

The thermal conditions of the heat sources in the systems in Fig. 1(a) can be measured by the values of the local and surface average heat transfer coefficients along the exposed heat source surfaces as well as the heat source temperatures and system/opening flow rates. The values of these measures at the "periodic" numerical solutions in a system employing the combined method can be used to indicate the impact of the combined method on the cooling of the heat sources. In this work, the cooling effect of the combined method is defined as the improvement in the time-averaged measures described above during the plate oscillations relative to those for an equivalent system with an opening but with no plate (acronym used—SSWONP). In addition, the effect of the relative positioning of the plate, heat sources, and opening as well as the values of the oscillation and clearance parameters on the cooling potential can be examined. This is achieved by analyzing the variation in the time averaged or cycle averaged values of the stated measures among the cases with the different parameters and system configurations as well as by comparing the measure values to those at steady state (1) in an equivalent system with an opening and no plate (SSWONP) and (2) in an equivalent system with no opening and no plate (acronym used—SSNONP).

The following set of assumptions and specifications is also followed in this investigation. Considering a channel of large depth, two-dimensional flow and temperature field assumptions are made. The flow in the system is laminar. Air, the cooling fluid, is assumed to be Newtonian and incompressible with constant and uniform properties excluding its density in the weight force of the momentum equations where the variation in the air density with temperature is modeled using the Boussinesq approximation. The properties of the solids involved are constant and uniform as well, with conduction in all solids modeled. The viscous dissipation, radiation, and internal heat generation in the fluid are negligible in comparison to the heat source heat rates [19].

Table 1
Parameter values

Parameters	
k (thermal conductivity of air)	$0.027\ \mathrm{W\,m^{-1}K^{-1}}$
ν (kinematic viscosity of air)	$1.717\times10^{-05}\ \mathrm{m\,s^{-2}}$
ρ (density of air)	$1.12492\ \mathrm{kg\,m^{-3}}$
c_p (specific heat of air)	$1005.93\ \mathrm{J\,kg^{-1}\,K^{-1}}$
β (volumetric expansion)	$1/315.5\ \mathrm{K^{-1}}$
k (thermal conductivity of heat sources, plate)	$177\ \mathrm{W\,m^{-1}\,K^{-1}}$
c_p (specific heat of heat sources, plate)	$875\ \mathrm{J\,kg^{-1}\,K^{-1}}$
ρ (density of heat sources)	$2770\ \mathrm{kg\,m^{-3}}$
k (thermal conductivity of board)	$0.26\ \mathrm{W\,m^{-1}\,K^{-1}}$
c_p (specific heat of board)	$1173\ \mathrm{J\,kg^{-1}\,K^{-1}}$
ρ (density of board)	$1207\ \mathrm{kg\,m^{-3}}$
System parameter	**Value**
g (gravitational acceleration)	$9.81\ \mathrm{m\,s^{-2}}$
T_o (ambient temperature)	25 °C
Q'''_a (applied volumetric heat generation rate)	$702.99\times10^{3}\ \mathrm{W\,m^{-3}}$
Gr (Grashof number based on b)	1160
Dimensional parameter[a]	**Value**
$b = L_{ref}$ (length basis)	0.25 in = 0.0635 m
BL = BH (heat source length and height)	b
BT (board thickness)	0.2b
CHL, CHU (channel heights)	2b
TL (channel length)	14b
SL (location of the first heat source)	5.5b
SPACE (spacing between heat sources)	0.50b
HW (width of the hole)	0.80b
PT (plate thickness)	0.2b
Case C	
S2 (spacing between plate and first heat source)	1.00b
PL (plate length)	0.75b
CM (plate clearance)	0.30b
Case D	
PL (plate length)	0.50b
CM (plate clearance)	0.50b
Case E	
PL (plate length)	0.75b
CM (plate clearance)	0.30b
Case F	
PL (plate length)	0.75b
CM (plate clearance)	0.30b

[a] Dimensions defined in Fig. 1(b).

2.1. Governing equations in dimensionless forms

The appropriate dimensionless forms of the continuity equation, the Navier–Stokes equations, and the energy equation are used to numerically determine the coupled velocity field, $u(x,y,t)$, $\mathrm{v}(x,y,t)$, pressure field, $p(x,y,t)$, and temperature field, $T(x,y,t)$. (A more comprehensive discussion is given in Florio [19].)

The set of dimensionless variables below is applied:

$$\tilde{x}_F = x/L_{ref}, \qquad \tilde{y}_F = y/L_{ref}$$
$$\tilde{g}_{comp_F} = g_{comp}/g, \qquad \widetilde{P}_F = P_D/P_{ref}$$
$$\tilde{u}_F = u/U_{ref}, \qquad \tilde{\mathrm{v}}_F = \mathrm{v}/U_{ref}, \qquad \tilde{t}_F = t/t_{ref}$$
$$\widetilde{Q}'''_F = Q'''_a/Q'''_{ref}, \qquad \widetilde{T}_F = (T-T_o)/\Delta T_{ref} \tag{2}$$

with

$$L_{ref} = \mathrm{BH} = b, \qquad U_{ref} = \sqrt{L_{ref} g\beta\Delta T_{ref}}$$
$$P_{ref} = L_{ref} g\beta\rho\Delta T_{ref}, \qquad t_{ref} = L_{ref}/U_{ref}$$
$$Q'''_{ref} = Q'''_a, \qquad \Delta T_{ref} = (Q'''_{ref}/\rho c_p)^{\frac{2}{3}}(L_{ref}/\beta g)^{\frac{1}{3}} \tag{2a}$$

For the systems in Fig. 1(a): For the fluid, the dimensionless form of the continuity equation is:

$$\frac{\partial\tilde{u}_F}{\partial\tilde{x}_F} + \frac{\partial\tilde{\mathrm{v}}_F}{\partial\tilde{y}_F} = 0 \tag{3}$$

The dimensionless x component of the momentum equation is:

$$\left(\frac{\partial\tilde{u}_F}{\partial\tilde{t}_F} + \tilde{u}_F\frac{\partial\tilde{u}_F}{\partial\tilde{x}_F} + \tilde{\mathrm{v}}_F\frac{\partial\tilde{u}_F}{\partial\tilde{y}_F}\right) = -\frac{\partial\tilde{p}_F}{\partial\tilde{x}_F} + \frac{1}{\sqrt{Gr}}\left(\frac{\partial^2\tilde{u}_F}{\partial\tilde{x}_F^2} + \frac{\partial^2\tilde{u}_F}{\partial\tilde{y}_F^2}\right) + \widetilde{T}_F \tag{4}$$

The dimensionless y component of the momentum equation becomes:

$$\left(\frac{\partial\tilde{\mathrm{v}}_F}{\partial\tilde{t}_F} + \tilde{u}_F\frac{\partial\tilde{\mathrm{v}}_F}{\partial\tilde{x}_F} + \tilde{\mathrm{v}}_F\frac{\partial\tilde{\mathrm{v}}_F}{\partial\tilde{y}_F}\right) = -\frac{\partial\tilde{p}_F}{\partial\tilde{y}_F} + \frac{1}{\sqrt{Gr}}\left(\frac{\partial^2\tilde{\mathrm{v}}_F}{\partial\tilde{x}_F^2} + \frac{\partial^2\tilde{\mathrm{v}}_F}{\partial\tilde{y}_F^2}\right) \tag{5}$$

The energy equation for the fluid in dimensionless form can be written as:

$$\left(\frac{\partial\widetilde{T}_F}{\partial\tilde{t}_F} + \tilde{u}_F\frac{\partial\widetilde{T}_F}{\partial\tilde{x}_F} + \tilde{\mathrm{v}}_F\frac{\partial\widetilde{T}_F}{\partial\tilde{y}_F}\right) = \frac{1}{Pr\sqrt{Gr}}\left(\frac{\partial^2\widetilde{T}_F}{\partial\tilde{x}_F^2} + \frac{\partial^2\widetilde{T}_F}{\partial\tilde{y}_F^2}\right) \tag{6}$$

For a solid generating heat, i.e. the heat sources, indicated by the subscript 1, the dimensionless energy equation takes the form:

$$\frac{\rho_1 c_{p1}}{\rho c_p}\frac{\partial\widetilde{T}_F}{\partial\tilde{t}_F} = \frac{k_1}{k\,Pr\sqrt{Gr}}\left(\frac{\partial^2\widetilde{T}_F}{\partial\tilde{x}_F^2} + \frac{\partial^2\widetilde{T}_F}{\partial\tilde{y}_F^2}\right) + \widetilde{Q}'''_F \tag{7}$$

For the solids with no internal heat generation, i.e. the board and plate, indicated by the subscript 2, the dimensionless energy equation is:

$$\frac{\rho_2 c_{p2}}{\rho c_p}\frac{\partial\widetilde{T}_F}{\partial\tilde{t}_F} = \frac{k_2}{k\,Pr\sqrt{Gr}}\left(\frac{\partial^2\widetilde{T}_F}{\partial\tilde{x}_F^2} + \frac{\partial^2\widetilde{T}_F}{\partial\tilde{y}_F^2}\right) \tag{8}$$

The dimensionless oscillation displacement from the mean clearance spacing can be expressed as:

$$\tilde{d}_{osF}(\tilde{t}_F) = (A/L_{ref})\sin(\tilde{\omega}_F\tilde{t}_F) \quad \text{with } \tilde{\omega}_F = \omega L_{ref}/U_{ref} \tag{9}$$

where $\tilde{\omega}_F$ is the dimensionless oscillation frequency and recall $L_{ref} = b$.

In the remainder of this work

$$A/b \text{ will be denoted by } d \quad \text{and} \quad \tilde{\omega}_F \text{ is denoted by } \omega \tag{10}$$

2.2. Initial and boundary conditions assigned

For each parameter case and system arrangement, the initial temperature and velocity fields are those at steady state with the plate fixed at its mean position in a system with the board opening (acronym used—SSWOWP).

The dimensionless boundary conditions applied are listed below with further explanation in [19].

At all solid and channel wall surfaces excluding those of the oscillating plate,

$$\tilde{u}_F = 0, \qquad \tilde{v}_F = 0 \tag{11a}$$

In the moving plate

$$\tilde{u}_F = 0, \qquad \tilde{v}_F = \mathrm{d}(\tilde{d}_{osF})/\mathrm{d}\tilde{t}_F \tag{11b}$$

A constant and uniform volumetric heat rate is applied to each heat source:

$$\widetilde{Q}'''_F = 1 \quad \text{within each heat source} \tag{12a}$$

A "conservative estimate" [23] of the possible cooling effect is made by applying an adiabatic condition to the end edges of the board (dimension symbols below defined in Fig. 1(b)):

$$\text{For } 0 > \tilde{y}_F > -\mathrm{BT}/b \quad \text{at} \quad \tilde{x}_F = 0 \quad \text{and}$$
$$\tilde{x}_F = \mathrm{TL}/b \qquad \partial\widetilde{T}_F/\partial\tilde{x}_F = 0 \tag{12b}$$

and an adiabatic condition to the upper and lower bounding channel surfaces:

$$\text{At } \tilde{y}_F = \mathrm{CHU}/b \quad \text{and} \quad \tilde{y}_F = -(\mathrm{CHL}+\mathrm{BT})/b$$
$$\partial\widetilde{T}_F/\partial\tilde{y}_F = 0 \tag{12c}$$

The flow and temperatures at the fluid/surroundings boundaries at $\tilde{x}_F = 0$ and $\tilde{x}_F = \mathrm{TL}/b$, which cannot be predetermined [24], are handled as indicated in Eq. (13) with the x component of velocity, $\tilde{u}_F$, through these surfaces then satisfying the conservation equations.

$$\text{At } \tilde{x}_F = 0, \quad \tilde{x}_F = \mathrm{TL}/b \quad \tilde{p}_F = 0 \tag{13a}$$

$$\text{At } \tilde{x}_F = 0, \quad \begin{cases} \tilde{u}_F \geq 0 \left\{ \widetilde{T}_F = \tilde{v}_F = 0 \right. \\ \tilde{u}_F < 0 \left\{ \partial\widetilde{T}_F/\partial\tilde{x}_F = \partial\tilde{v}_F/\partial\tilde{x}_F = 0 \right. \end{cases}$$
$$\text{At } \tilde{x}_F = \mathrm{TL}/b, \quad \begin{cases} \tilde{u}_F \leq 0 \left\{ \widetilde{T}_F = \tilde{v}_F = 0 \right. \\ \tilde{u}_F > 0 \left\{ \partial\widetilde{T}_F/\partial\tilde{x}_F = \partial\tilde{v}_F/\partial\tilde{x}_F = 0 \right. \end{cases} \tag{13b}$$

2.3. Calculated parameters

In this investigation, the dimensionless form of the local heat flux is given by:

$$\tilde{q}_F = q/q_{ref} = -\left(1/(Pr\sqrt{Gr})\right)(\partial\widetilde{T}_F/\partial\tilde{n}_F)$$
$$\text{where } q_{ref} = Q'''_{ref} L_{ref} \tag{14}$$

The dimensionless heat transfer coefficient is defined as:

$$\tilde{h}_F = h/h_{ref} = \tilde{q}_F/\widetilde{T}_F \quad \text{where } h_{ref} = k\,Pr\sqrt{Gr}/L_{ref} \tag{15}$$

2.4. Implementation of finite element method

The finite element investigations that determine the heat and fluid flow in the various systems were performed using a commercially available finite element program FIDAP©. (Further details about the solution procedures and the "elasticity based remeshing" used to model the plate motion are available

Table 2
Summary of steady state results

a. Dimensionless temperatures and heat transfer coefficients

Case[a]	Max Vel	Max $\widetilde{T}_F$		Surface average $\tilde{h}_F$					
		H1	H2	H1L	H1T	H1R	H2L	H2T	H2R
Standard – no plate	2.862	1.7581	1.9576	0.1246	0.1352	0.0482	0.1201	0.0838	0.0351
No plate or opening	2.497	1.8806	1.9687	0.1303	0.1457	0.0233	0.0559	0.1362	0.0390
A – Plate over source 2	2.59	1.8867	2.3806	0.1174	0.1285	0.0361	0.0682	0.0966	0.0291
B – Plates over source 1 and 2	2.871	1.8806	1.9687	0.1051	0.1165	0.0467	0.1215	0.0818	0.0278
C – Plate upstream of heat sources	2.841	1.7318	1.8832	0.1342	0.1263	0.0493	0.1308	0.0832	0.0348
D – Plate over opening	2.665	1.7927	2.2838	0.1284	0.1411	0.0396	0.0738	0.0987	0.0371
E – Plate over opening at level of top of sources	2.898	1.8162	2.1154	0.1194	0.1300	0.0456	0.1039	0.0795	0.0334
F – Plate over source 1	3.015	1.7604	1.7113	0.1111	0.1289	0.0496	0.1613	0.0779	0.0348

Dimensionless flow rates through upper and lower channels

Config	In upper	In lower	Out upper	Out lower	Opening[b]
No opening – no plate	1.578	2.118	1.578	2.1187	N/A
Opening – no plate	1.326	2.565	1.953	1.938	0.627
Case A	1.040	2.274	1.294	2.021	0.253
Case B	0.665	1.294	1.362	0.696	0.696
Case C	1.221	2.682	1.937	1.966	0.716
Case D	1.500	2.217	1.744	1.974	0.243
Case E	1.126	2.408	1.587	1.947	0.461
Case F	0.849	3.265	1.861	2.258	1.012

[a] Geometry Fig 1(a). L, R and T refer to the left, right and top surfaces of heat source 1 (H1) or heat source 2 (H2).
[b] from lower channel to upper channel.

in [19,25].) Compromises between the computational requirements (run time and storage) and accuracy lead to a 337 × 217, 9 node-quadrilateral finite element mesh of the model geometry with more elements assigned near the inlet, the channel walls, the board and heat source surfaces, and the moving plate to more accurately capture the temperature and velocity. A mesh sensitivity study showed further mesh refinement caused at most a 0.5% change in the predicted results. The small time steps ranging from 5×10^{-05} to 5×10^{-04} needed for convergence, the large number of nodes, the coupling of the governing equations, and the remeshing scheme modeling the plate motion limited the total number of parameter sets studied.

At a given time step, a segregated solution procedure was used to determine the flow and temperature fields from the set of equations that form the finite element discretizations of the governing equations. Convergence of the nodal values of the dependent variable, ψ, at each time step is reached when $\|(\psi_i - \psi_{i-1})/\psi_i\| \leq 10^{-03}$, where ψ denotes any dependent variable ($\tilde{u}_F, \tilde{v}_F, \widetilde{T}_F$, or $\tilde{p}_F$), $\| \ \|$ stands for the root mean square norm summed over all ψ nodes, and i is the solution iteration count. A "periodic" solution is attained when the cycle averages of each of the heat source surface average heat transfer coefficients, the local heat transfer coefficients at the four points on each heat source indicated in Fig. 1(a), and the maximum system temperature and velocity for the current oscillation differ by less than 0.10% from their respective cycle averages over the previous oscillation.

3. Results

The effectiveness of the combination method can be determined by comparing the conditions that result with the combination method to those that develop for pure natural convection. Therefore, the discussion of results begins with a brief description of the steady state natural convection flow and temperature fields before proceeding to the transient results with the vibrating plate. The clearance referred to in the text indicates the region between the bottom surface of the fixed plate and an offset distance of CM below the plate for steady state-fixed plate conditions and the instantaneous region between the bottom of the moving plate and an offset distance $C(t)$ below the plate as labeled in Fig. 1(a) for transient-oscillating plate conditions. Top, bottom, left and right mentioned are the orientations with respect to the associated figures.

3.1. Steady state natural convection cooling with and without a cross-flow opening or fixed plate

A number of steady state temperature and velocity fields for a system with two heat sources were determined to establish a baseline from which to gauge the effectiveness of the plate oscillation-cross-flow combination as well as to assist in the selection of the configurations for which studies with the oscillating plate are to be carried out. The steady state configurations investigated include a system with no opening and no moving plate (SSNONP), a system with the opening, but with no plate (SSWONP), and finally a sequence of systems with an opening as well as a fixed plate (SSWOWP) located at the positions listed in Table 2. For all of the steady state systems described above, a "main" channel natural convection induced flow develops in the upper channel, defined in Fig. 1(a), which contains the heat sources, and in the lower channel, defined in Fig. 1(a), below the heat sources. These channel flows carry the heat and fluid from left to right around the flow obstacles in the channel. In the case of a cross-flow opening, the natural convection effects also induce the cross-flow through the board opening as described in [19]. The "main" channel natural convection flow rates and the amount of and flow paths of the cross-flow differ with the geometric configurations, i.e. the presence and relative positioning of the board opening or fixed plate. Therefore, the temperature fields will vary with these conditions as well. The major results are summarized in Table 2.

In a system with no opening and no plate, the thermal conditions in the region between the two heat sources are very poor with the temperature of the heat source 2, to the right, being higher than the temperature of the heat source 1 on the left. These characteristics are apparent in the values and spacing of the temperature contours shown in Fig. 2(a). The passage of the cross-flow in the area between the heat sources when a board opening is present significantly reduces the size and magnitude of the high temperature zones (Fig. 2(b)). For the parameters investigated, the average temperature of heat source 2 decreases by 16% from that in an equivalent system without the opening, and the heat transfer coefficient from its left side surface improves by 114%.

The system configurations in Table 2 for which steady state studies with a fixed plate were performed were selected for their potential to draw fluid through the opening, to promote laminar thermal mixing of fluid in the region between the heat sources, and to generally increase the velocities/velocity gradients near the heated surfaces. Transient analyses were then pursued only for those arrangements for which:

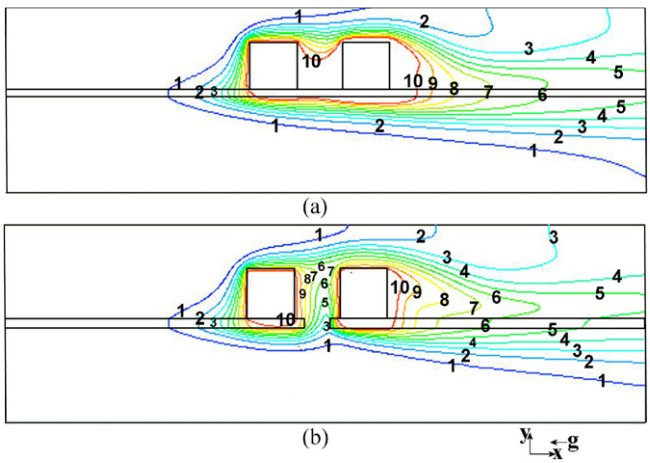

Fig. 2. Contours of steady state dimensionless temperature, $\widetilde{T}_F$: (a) no plate – no opening; (b) opening – no plate. Value of temperature of contour labeled M is 0.0875[2M-1]. $\widetilde{T}_F$ defined in Eq. (8).

(1) the steady state results with the fixed or non-moving plate showed the presence of the plate improved the thermal conditions in some portion of the system,
(2) the results of the previous studies of the effects of solely the plate oscillations suggest the potential for oscillation induced improvement despite the flow constriction the plate may cause.

Based on these criteria, further studies were not pursued for the case A arrangement, with the plate placed over heat source 2, and the case B arrangement, with a plate placed over each of the heat sources (two plate arrangement) (see Table 2). The case A configuration severely reduces the cross-flow (60%) and significantly increases the operating temperature of heat source 2 (21%) from the opening-no plate conditions (SSWONP). The case B arrangement results in considerable constriction of the channel flow from SSWONP (50% decrease in the flow entering upper channel, 30% exiting). The resulting reductions in the heat transfer, especially from some side surfaces of the heat sources, cannot be easily recovered by the oscillations of a plate near the tops of the heat sources. Hence, for these two arrangements, the potential for the oscillation/cross-flow induced enhancement relative to SSWONP conditions is minimal.

The remaining four configurations showed greater promise. The placement of the plate to the left of heat source 1, the case C geometry (Fig. 1(a)), produces the least resistance to the flow moving around the heat sources among the arrangements studied and actually leads to an increase in the opening flowrate (Table 2). The change in the flow patterns causes at least a 3.5% reduction in the average temperature of the heat sources compared with SSWONP. Transient studies were undertaken for this configuration.

The plate positioning in the three remaining configurations produces a greater constriction of the flow near the heat sources than in the case C geometry and hence significant improvement in the thermal conditions for the steady state fixed plate conditions is not observed. However, the oscillations of the plate at these three locations have a high potential to benefit the thermal conditions of the heat sources in light of the previous studies of the effects of solely the plate oscillations [19].

The positioning of a fixed plate in the "cavity" space between the heat sources in the case D arrangement (Fig. 1(a)), restricts the opening through-flow by 61% from SSWONP despite a relatively large mean clearance spacing, CM. The decrease in this flow is partially compensated for by the increased inflow into the upper channel which contains the heat sources. As a result, the surface average heat transfer coefficients at the interior side (cavity) surfaces decrease by as much as 38% relative to those for SSWONP conditions, though the surface average coefficients at all exterior heat source surfaces increase (maximum of 18% on the top of heat source 2). The oscillations of the plate in the case D arrangement are expected to locally increase the velocities and thus the local heat flow near the side cavity surfaces, thereby enhancing the general cooling of the heat sources even with the reduced opening flow.

In the case E arrangement (Fig. 1(a)), the plate is placed just over the cavity between the heat sources at the level of the top of the heat sources and so is within the path of the main upper channel flow over the heat sources as well as the opening flow, but is less restrictive of the opening flow than case D. In this case E arrangement, the flowrate entering the upper channel is reduced by 15% and the flow through the opening decreases by only 27% relative to those at SSWONP. The steady state flow patterns cause the surface average heat transfer coefficients at all exposed heat source surfaces to decrease by about 5% or less except at the left side of heat source 2 where the diminished opening flow causes a 15% drop (Table 2). Hence, with this arrangement, the opening flow is better able to contribute to improving the heat flow from the fluid near the heat sources than case D, and the interaction of the opening flow with the flow streams generated by the plate oscillations has the potential to further augment the cooling particularly at the interior heat source side surfaces and at the top of heat source 2.

The most improved steady state heat source thermal conditions among the final three configurations occurred with the plate centered over the top of heat source 1 (case F in Fig. 1(a)). This position poses the least restriction to the cooler opening flow streams brought to the heat source area. In fact, the opening flow is 60% higher than that at SSWONP and comprises about 52% of the flow exiting the upper channel. Hence, while the upper channel inflow decreases by 35%, with the fixed plate, the outflow is only 5% lower than that with solely the opening. The increased opening flow can be attributed to the larger pressure difference between the region near the tops of the heat sources and the area near the board opening caused by the presence of the plate. In response, the average temperature of heat source 2 decreases by 13% relative to the SSWONP configuration (Table 2). The plate oscillations can help improve the cooling of mainly heat source 1 by increasing the local velocities near the top of this heat source. The conditions of heat source 2 can benefit from the alteration in the paths of the opening flow and the flow moving over heat source 2 caused by the plate and its oscillations with little impedance to the opening flow rate.

3.2. *Active natural convection enhancement—vibrating plate and cross-flow*

Thus, the oscillatory motion of the plate can be used to adjust the flows over the heat sources and, by doing so, to manipulate the thermal conditions in the system. The higher the natural convection–opening–oscillation induced velocities and velocity gradients near the heat sources relative to those at the equivalent steady state conditions, the greater the potential for localized cooling. The discussion of the transient results explores the effects of the oscillation/clearance parameters and plate positioning on the system velocity distribution and thus the heat transfer enhancement capabilities. Unless otherwise indicated, all results presented and summarized in Table 3 refer to the time averaged "periodic" solution values over one plate oscillation.

Table 3
Summary of time (cycle) average dimensionless results at transient steady state

	Max $\widetilde{T}_F$	Surface average $\tilde{h}_F$			Local $\tilde{h}_F$			
		Left	Top	Right	Point 1	Point 2	Point 3	Point 4
Heat source 1								
SS without plate	1.758	0.1246	0.1352	0.04819	0.0999	0.1333	0.1095	0.04346
SS without plate without opening	1.847	0.1303	0.1457	0.02327	0.1040	0.1410	0.1200	0.00908
Case C arrangement	CM/$b = 0.3$							
SS with plate	1.732	0.1342	0.1263	0.04932	0.1109	0.1224	0.1020	0.04492
$d = 0.20$ $\omega = 4\pi$	1.732	0.1320	0.1208	0.04946	0.1096	0.1139	0.1003	0.04459
$d = 0.20$ $\omega = 8\pi$	1.732	0.1354	0.1228	0.04940	0.1156	0.1110	0.1024	0.04518
Case D arrangement	CM/$b = 0.5$							
SS with plate	1.793	0.1284	0.1411	0.03960	0.1027	0.1383	0.1154	0.03847
$d = 0.20$ $\omega = 2\pi$	1.793	0.1288	0.1409	0.03732	0.1030	0.1384	0.1152	0.03325
$d = 0.20$ $\omega = 4\pi$	1.793	0.1292	0.1417	0.03860	0.1033	0.1388	0.1162	0.03698
Case E arrangement	CM/$b = 0.3$							
SS with plate	1.816	0.1194	0.1300	0.04564	0.0967	0.1265	0.1044	0.03772
$d = 0.10$ $\omega = 2\pi$	1.816	0.1191	0.1298	0.04577	0.0965	0.1264	0.1041	0.03779
$d = 0.20$ $\omega = 2\pi$	1.816	0.1191	0.1294	0.04634	0.0964	0.1264	0.1039	0.03847
Case F arrangement	CM/$b = 0.3$							
SS with plate	1.760	0.1111	0.1289	0.04961	0.0903	0.1417	0.1012	0.04679
$d = 0.20$ $\omega = 2\pi$	1.761	0.1090	0.1711	0.05811	0.0892	0.1847	0.1553	0.04782
$d = 0.20$ $\omega = 4\pi$	1.761	0.1099	0.1993	0.05878	0.0890	0.1983	0.1862	0.04737
Heat source 2								
SS without plate	1.958	0.1201	0.0838	0.03510	0.1090	0.0766	0.0733	0.02831
SS without plate without opening	2.355	0.0559	0.1362	0.03901	0.0268	0.1315	0.1167	0.02813
Case C arrangement	CM/$b = 0.3$							
SS with plate	1.883	0.1308	0.0832	0.03483	0.1213	0.0765	0.0716	0.02808
$d = 0.20$ $\omega = 4\pi$	1.884	0.1313	0.0833	0.03478	0.1205	0.0773	0.0732	0.02826
$d = 0.20$ $\omega = 8\pi$	1.884	0.1315	0.0826	0.03487	0.1230	0.0752	0.0713	0.02813
Case D arrangement	CM/$b = 0.5$							
SS with plate	2.2838	0.0738	0.0987	0.03715	0.0703	0.0904	0.0924	0.02831
$d = 0.20$ $\omega = 2\pi$	2.2841	0.0749	0.1010	0.03721	0.0663	0.0926	0.0943	0.02830
$d = 0.20$ $\omega = 4\pi$	2.2841	0.0802	0.0984	0.03694	0.0796	0.0907	0.0922	0.02828
Case E arrangement	CM/$b = 0.3$							
SS with plate	2.115	0.1039	0.0795	0.03344	0.0902	0.0718	0.0715	0.0253
$d = 0.10$ $\omega = 2\pi$	2.115	0.1036	0.0860	0.03516	0.0897	0.0739	0.0800	0.0256
$d = 0.20$ $\omega = 2\pi$	2.116	0.1024	0.1076	0.03884	0.0884	0.0924	0.1046	0.0261
Case F arrangement	CM/$b = 0.3$							
SS with plate	1.711	0.1613	0.0778	0.03477	0.1529	0.0704	0.0669	0.02789
$d = 0.20$ $\omega = 2\pi$	1.711	0.1622	0.0781	0.03490	0.1546	0.0706	0.0655	0.0279
$d = 0.20$ $\omega = 4\pi$	1.711	0.1639	0.0782	0.03494	0.1572	0.0686	0.0686	0.0280

3.2.1. Oscillating plate to left of both heat sources—Case C

The first arrangement for which a transient analysis is undertaken is with the oscillating plate located to the left or upstream of both heat sources (case C in Fig. 1(a), dimensioning in Fig. 1(b)). While the positioning of the plate "far" from the heat sources produces minimal constriction of the flow around the heat sources and generally improves the thermal conditions slightly over those for SSWONP, the potential impact of the oscillations on the velocity field near the heat sources is diminished for the parameter set studied. This is clearly seen in Fig. 3 where the greatest intensity of the oscillation induced flows (area c in Fig. 3(a)) and thus the oscillation based cooling potential are found in the immediate vicinity of the vibrating plate. Though a wide range of displacement amplitudes (from 0.05 to 0.20) and oscillation frequencies (between 2 and 8π) were tested after selecting the $S2$ dimension that limits the constriction of the flow over the heat source, the only noticeable impact of the oscillations is the slight change in the velocity and temperature distributions near the top left corners of both heat sources (area a in Fig. 3(a) for example) for dimensionless dis-

placement amplitudes of 0.20 and higher-end frequency values. The flow near heat source 1 changes as a direct result of the flows created by the plate motion which are carried to the right with the natural convection channel flow, and heat source 2 feels the effects of the resulting variation in the opening flow. See Electronic Annex 1 in the online version of this article for the velocity distribution for the case with $d = 0.20$, $\omega = 8\pi$ and Electronic Annex 2 for an animation of the corresponding temperature field as well as Fig. 3. Fig. 4 shows the transient local heat transfer coefficients for the same case.

The thermal conditions of the heat sources are most affected in the areas where the combination method produces the greatest changes in the velocity field. Hence, investigating the local heat transfer coefficient at the four representative positions on each of the heat sources as marked in Fig. 1(a) will help in the understanding of the cooling potential with the case C arrangement. For the parameters investigated for this arrangement, the combination natural convection–opening–oscillation method is of most benefit to heat source 1 at point 1 on its left side (Fig. 1(a)). The higher oscillation induced velocities near this location (area a in Fig. 3(a)) result in as much as a 16% increase in the local heat transfer coefficient relative to that at SSWONP (Table 3, Electronic Annexes 1, 2). The diversion of flow from the top of the heat source (area b in Fig. 3(a)) caused by the increased velocities impinging on the left side of this heat source lead to, at a minimum, a 16% and 6% decrease in the heat transfer coefficients at points 2 and 3 on the top of the heat source, respectively, from those at SSWONP. The greatest variation in the heat transfer coefficient with time among the four points considered on heat source 1 occurs at point 2 as seen in Fig. 4(a). This results from the periodic flow diversion from the top of this heat source at area b in Fig. 3(a) during the plate oscillations. The combination of the oscillations and the opening flow has a lesser effect on the right side of heat source 1, such as at point 4, where the maximum increase in the local heat transfer coefficient is 4%.

Since heat source 2 is even further from the moving plate, the heat transfer coefficients at heat source 2 do not change significantly with time as is clear in Fig. 4(b) and the results in Table 3. The greatest alteration in the local heat transfer coefficient on heat source 2 from the SSWONP conditions occurs near the point 1 area where the local heat transfer coefficient experiences a 12% increase. A maximum 21% increase in the net opening flow relative to no plate conditions caused mainly by the changes in the flow paths resulting from the presence of the plate alone, not its motion, is the reason for this rise and demonstrates the minimal influence of the plate oscillations on the conditions at heat source 2. The other three points examined on this heat source experience less than a 3% change from SSWONP (Table 3, Fig. 4(b)). As with all cases with significant opening cross-flow, the flow is directed away from the top

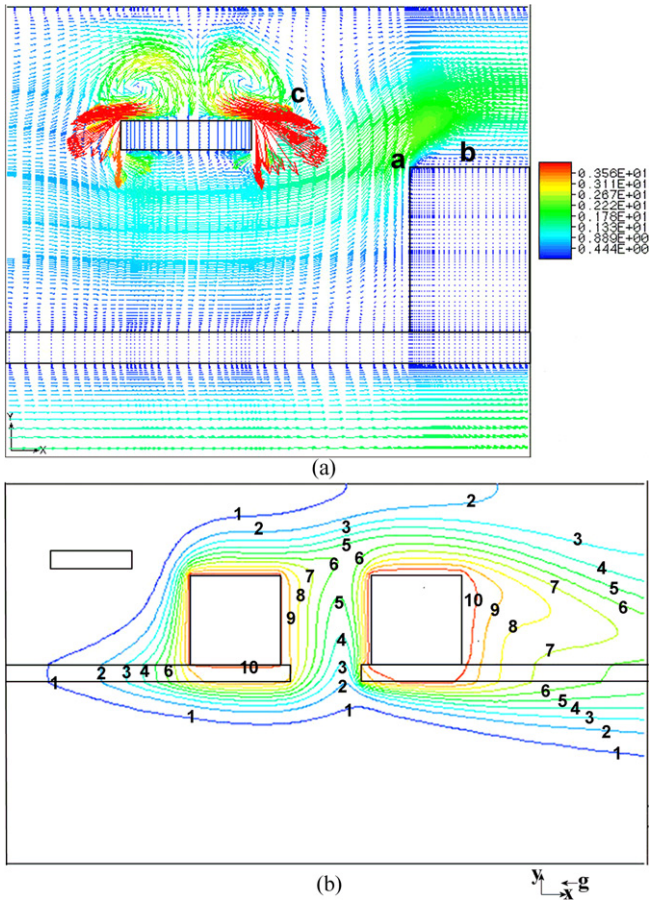

Fig. 3. Sample results for case C arrangement with $d = 0.20$, $\omega = 8\pi$, CM/$b = 0.30$ at $\tilde{t}_F = 0.94$: (a) vector plot of dimensionless velocity field $[\tilde{u}_F, \tilde{v}_F]$ defined in Eq. (8) near moving plate. Vector length and color are indicators of velocity magnitude; (b) Contours dimensionless temperature, $\widetilde{T}_F$, near heat sources. Value of temperature of contour labeled M is 0.09[2M-1].

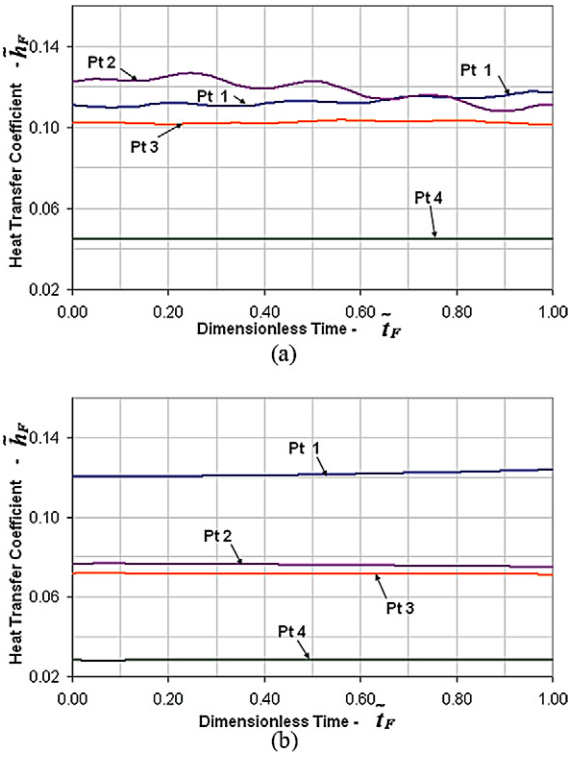

Fig. 4. Heat transfer coefficient, $\tilde{h}_F$, results for case C with $d = 0.20$, $\omega = 8\pi$, CM/$b = 0.30$: (a) Local $\tilde{h}_F$ heat source 1 at four points in Fig. 1(a).versus $\tilde{t}_F$; (b) Local $\tilde{h}_F$ heat source 2 at four points in Fig. 1(a) versus $\tilde{t}_F$.

of heat source 2 (which is downstream or to the right of the opening) which then reduces the heat removal from this area relative to conditions for which there is no opening. Hence, the heat transfer coefficients at points 2 and 3 on the top surface are approximately 40% lower than those in a system with no opening and no plate (SSNONP) (see Electronic Annex 1). Thus, the effects of the cross-flow through the opening and the plate position, not the oscillations, dominate the thermal conditions of the second heat source.

In summary, for the case C set-up, the relatively distant location of the plate from the heat sources suppresses the potential for oscillation-based cooling. Slight improvements at only limited heat source locations could be attributed to the oscillations. Instead, the cross-flow through the opening and the presence of the plate governed the overall thermal conditions of the heat sources, particularly at heat source 2. Based on these results, using the combination method with this arrangement does not appear to have the potential to bring about significant improvements in the thermal conditions of the heat sources.

3.2.2. *Oscillating plate just above opening—Case D*

In the second configuration, the plate is placed in the cavity between the heat sources (the area with the poorest thermal conditions without the cross-flow). The oscillations of a plate in such a position can be used particularly to enhance the mixing of the heated fluid near the interior side surfaces of the heat sources with the cooler opening flow (case D in Fig. 1(a), dimensioning follows from Fig. 1(b)). Also, the placement of the plate closer to the heat sources allows the oscillations to have a greater impact on the heat transfer from the heat sources than in the case C arrangement.

Over the parameters studied, the mean clearance value, CM, must be large enough to allow for a net cycle-averaged opening flow from the lower channel to the upper channel for the method to be of benefit. In addition, for a fixed clearance, the plate displacement amplitude was shown to be critical to the level of the cooling effect. For the clearance used in the results reported in this work, a dimensionless displacement of at least 0.20 was needed for a noticeable variation in the heat transfer coefficients along the top and interior side surfaces of the heat sources. The displacement and mean clearance are important factors governing not only the oscillation induced flow patterns but also the intensity and movement of the opening flow streams. Under the conditions of sufficient clearance and displacement amplitude, studies varying the oscillation frequency were performed with the related parameters and a summary of results presented in Tables 1 and 3 respectively. Though increasing the oscillation frequency causes more complex flow patterns, the cooling at the heat sources is not necessarily improved. See Electronic Annex 3 in the online version of this article for the velocity distribution with $d = 0.20$, $\omega = 4\pi$ and Electronic Annex 4 for an animation of the corresponding temperature field as well as Fig. 5. Fig. 6 shows the transient local heat transfer coefficients for the same case.

While the net cycle average flows for the cases studied moved fluid from the lower channel to the upper channel, instantaneous reverse flow did develop for the higher frequency case. The instantaneous flowrates were found to be higher for the higher frequency (plate velocity) case with a maximum flow from the lower channel to the upper channel of 23% of the SSWONP flow exiting the upper channel and a maximum reverse opening flow of at most 6% of this steady state flow. Minimal opening flow "reversal" occurred for the lower frequency case. The time averaged net opening flow was found to be higher for the lower frequency (plate velocity) case with a maximum value of 10% of the outflow from the upper channel at SSWONP.

The effects of the flow patterns resulting from the oscillations, the opening flow, and the natural convection on the heat source thermal conditions for the case D arrangement can be considered by analyzing the changes in the heat transfer coefficients along the heat sources relative to SSWONP. Of the four locations on heat source 1, the point 4 location, on the right side, experiences the largest variation in the local heat transfer coefficient over an oscillation in terms of intensity and amplitude. The strong oscillatory nature of the local point 4 coefficient can be attributed the changes in the local velocity field, with a typical distribution depicted in Fig. 5(a). The point 4 area is located in close proximity to the moving plate and so is near the periodically higher velocity streams (area c in Fig. 5(a)) and the alternately directed circulating zones (such as near area g in Fig. 5(a)) generated to the left of the plate. In addition, flow periodically passes over the top of heat source 1 and into the cavity between the heat sources (area a to area b in Fig. 5(a)) and is then periodically blocked. These flow streams can be identified over an entire plate oscillation in Electronic Annex 3. The transient and complex interaction of these flows gives rise to the heat transfer coefficient characteristics discussed. Despite the high velocity flow streams involved, the time averaged velocity near point 4 where these streams essentially coalesce is lower than that for SSWONP (Electronic Annex 3 and area b in Fig. 5(a)). Therefore, the time averaged heat transfer coefficient at point 4 is reduced by, at a minimum, 14% compared with SSWONP (Electronic Annex 4 and Fig. 5(b)). It is expected that at locations slightly below point 4, closer to area c in Fig. 5(a), where the higher plate induced velocities are more intense and tend to dominate the local flow field, the heat transfer coefficients are improved relative to SSWONP. The left and top heat source surfaces, which are upstream or to the left of the plate, experience only minimal effects of the plate motion with changes in the heat transfer coefficients at points 1 to 3 (Fig. 6(a)) ranging between 3 and 4% of the SSWONP conditions as the effects of the oscillations and the opening are carried to the right by the main channel flow.

The most complex variation in the thermal conditions on heat source 2, with the oscillation-opening combination, occurs on the left side surface as can be seen by the plot of the local coefficient at point 1 in Fig. 6(b) near area e in Fig. 5(a). Although the combination of the periodic opening through-flow, the flow generated by the plate motion (area d, h in Fig. 5(a)), and the channel flow in the upper channel create the complex flow patterns, a low velocity region typically results near the upper left corner of heat source 2, near point 1 close to area e in Fig. 5(a), similar to point 4 near area b on the first heat source (Electronic Annex 3, Fig. 5(a)). This results in at least a 26% decrease in

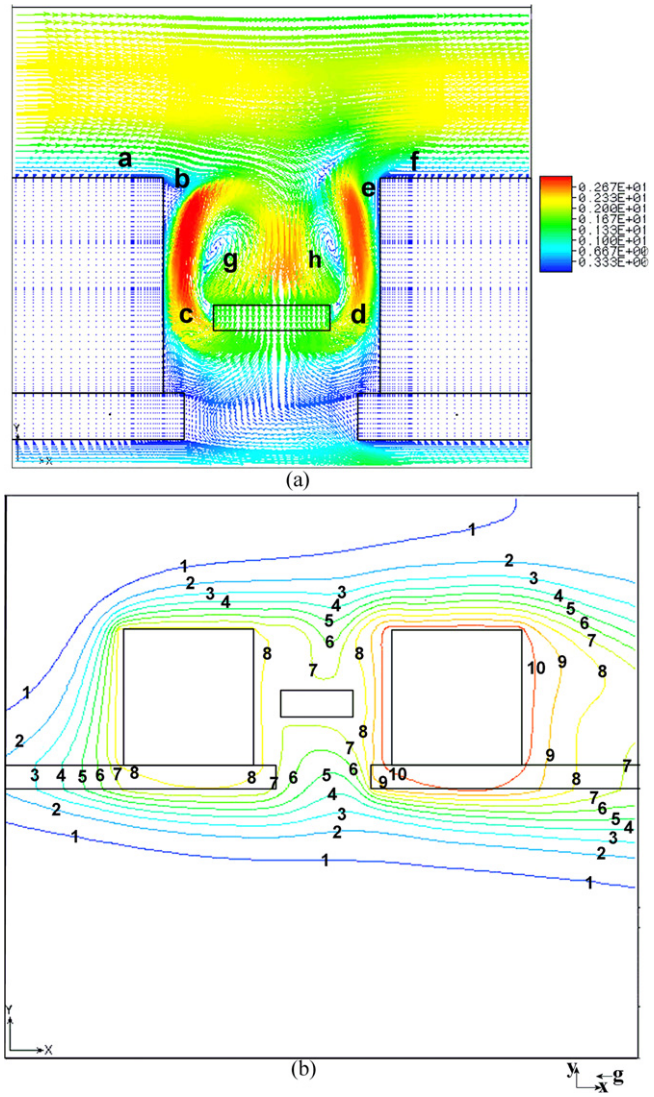

Fig. 5. Sample results near heat sources for case D arrangement with $d = 0.20$, $\omega = 8\pi$, CM/$b = 0.30$ at $\tilde{t}_F = 1.32$: (a) vector plot of dimensionless velocity field $[\tilde{u}_F, \tilde{v}_F]$; (b) Contours dimensionless temperature, $\widetilde{T}_F$: Value of temperature of contour labeled M is 0.1125[2M-1].

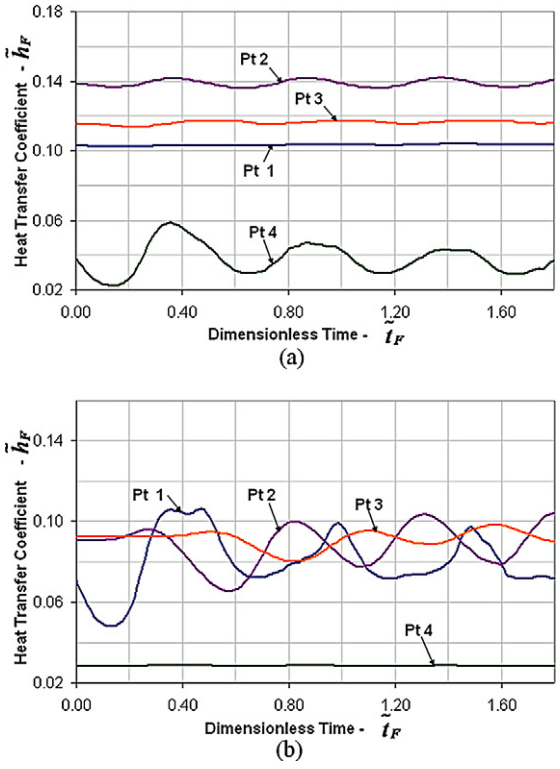

Fig. 6. Dimensionless heat transfer coefficient, $\tilde{h}_F$, results for case D with $d = 0.20$, $\omega = 8\pi$, CM/$b = 0.30$: (a) Local $\tilde{h}_F$ at four points indicated on heat source 1 in Fig. 1(a). versus dimensionless time; (b) Local $\tilde{h}_F$ at four points indicated on heat source 2 in Fig. 1(a) versus dimensionless time.

the heat transfer coefficient from that for the SSWONP configuration (Electronic Annex 4, and Figs. 5(b), 6(b)).

At the top of heat source 2, the changes in the flow paths and flowrates caused by the geometric arrangement of the plate, opening, and heat sources have a greater effect on the thermal conditions than the flow streams caused by the plate oscillations. The decreased opening flow rate with the plate positioned in the cavity area together with the restrictions in the available flow paths with the modified geometry cause a reduction in the diversion of the flow from the top of heat source 2 away from area f in Fig. 5(a) compared to that occurring under SSWONP conditions. This effect is, in part, responsible for the increase in the heat transfer coefficients at points 2 and 3 of a maximum of 18 and 26% from those for SSWONP respectively (Fig. 6(b), Electronic Annexes 3, 4). For increasing frequencies, the increased instantaneous opening flowrate and the accompanying increase in the flow deflection lead to lower heat transfer coefficients, illustrating that higher plate velocities are not always more beneficial to the cooling. Though the heat transfer coefficient values reported, especially for the lower frequency case, represent a significant increase relative to SSWONP, the SSWONP local top surface coefficient values are about 40% lower than those for a system with no plate and no opening (SSNONP) where there is no such flow deflection from the top of heat source 2 (Electronic Annexes 3, 4, and Figs. 5, 6(b)).

On the right side of the second heat source, at point 4, the changes in the velocity field and thus the heat transfer coefficients are minimal (Electronic Annexes 3, 4 and Figs. 5, 6(b)).

The oscillations for the case D configuration clearly have a greater influence on the velocities/heat flow near the heat sources than for case C. This is exemplified by the more complex flow patterns that develop and particularly the potential for heat transfer enhancement at the interior surfaces of the heat sources just near the ends of the moving plate. However, for the parameter sets investigated, the cooling augmentation possible with this method is limited by the general blockage of the opening flow caused by the presence of the plate and the ensuing velocity fields. Therefore, this case D arrangement is not recommended.

3.2.3. Oscillating plate above spacing between heat sources—top of heat source level—Case E

In the case E system configuration, the plate remains over the cavity between the heat sources, but is just level to the tops of the heat sources (Fig. 1(a)). This placement is designed to re-

duce the opening flow obstruction while still allowing the plate oscillations to significantly impact the flows and thus the heat transfer near the heat sources. The arrangement dimensions are shown in Fig. 1(b) and the results summarized in Table 3. The findings indicate that with this arrangement, the cooling effect generated, which occurs mainly on heat source 2, increases with the displacement amplitude for fixed clearance and oscillation frequency values. See Electronic Annex 5 in the online version of this article for the velocity distribution for the case with $d = 0.20$, $\omega = 2\pi$ and Electronic Annex 6 for an animation of the corresponding temperature distribution as well as Fig. 7. Fig. 8 depicts the local heat transfer coefficients for this sample case.

For the parameters tested with the case E arrangement, throughout a plate oscillation there is fluctuating but continual net and instantaneous flow from the lower channel to the upper channel. This net flow averaged over one oscillation is at maximum about 23% of the flow that exits the upper channel under conditions with no plate in the channel (SSWONP), with only a slight variation in the instantaneous flowrate, ranging between 18% and 27% of this steady state flow. The maintenance of a more consistent and higher opening through-flow over the course of an oscillation than for the case D arrangement is one of the primary reasons for the improved thermal conditions found with this E configuration, particularly at heat source 2.

To further the understanding of how the motion of the plate in this configuration, the opening flow, and the natural convection can be used to improve the thermal conditions of the heat sources, the typical velocities near the heat sources during a plate oscillation are reviewed. The description begins with the downward moving plate coming to a stop at its minimum clearance position. Just as the plate stops moving downward, fluid is being "squeezed" into the upper channel between the lower right corner of the plate and the left upper corner of heat source 2, producing a "jet-like" flow (area d in Fig. 7(a), and Electronic Annex 5). The then upward motion of the plate causes the higher velocity "jet-like" flow to pass over the top of heat source 2 near area e in Fig. 7(a). In the cavity between the heat sources, the general rightward movement of the opening flow, which partially feeds the "jet-like" flow, reduces the velocities near the right side of heat source 1, near area b in Fig. 7(a), from those at SSWONP. The increase in the clearance spacing

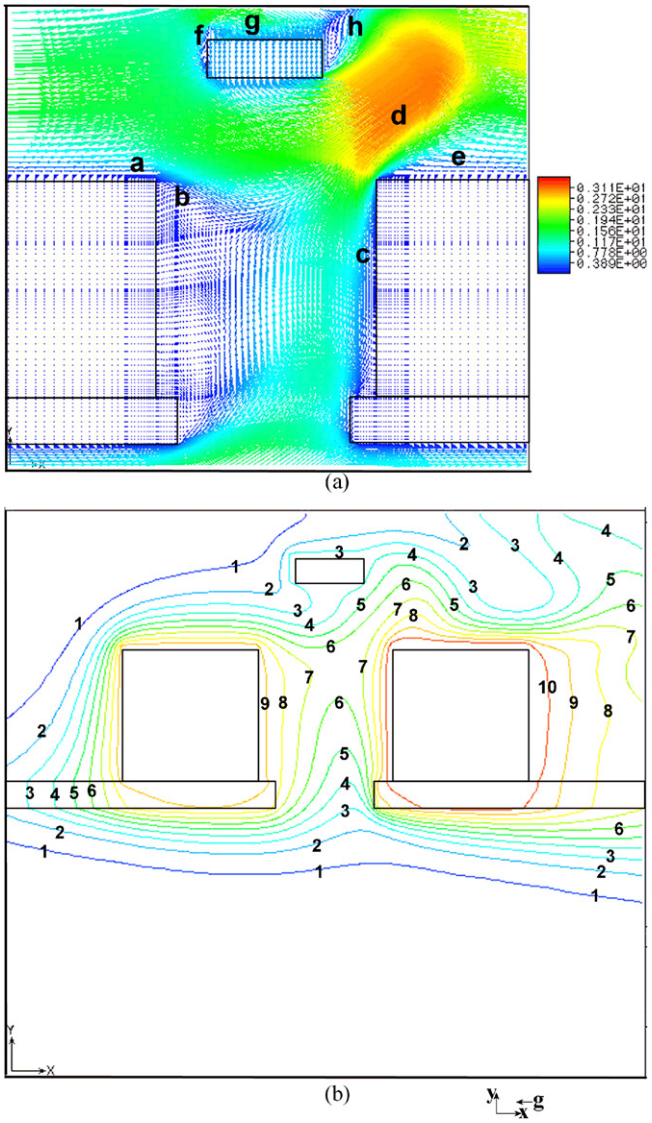

Fig. 7. Sample results near heat sources for case E arrangement with $d = 0.20$, $\omega = 2\pi$, CM/$b = 0.30$ at $\tilde{t}_F = 3.32$: (a) vector plot of dimensionless velocity field $[\tilde{u}_F, \tilde{v}_F]$; (b) Contours dimensionless temperature, $\tilde{T}_F$: Value of temperature of contour labeled M is 0.10[2M-1].

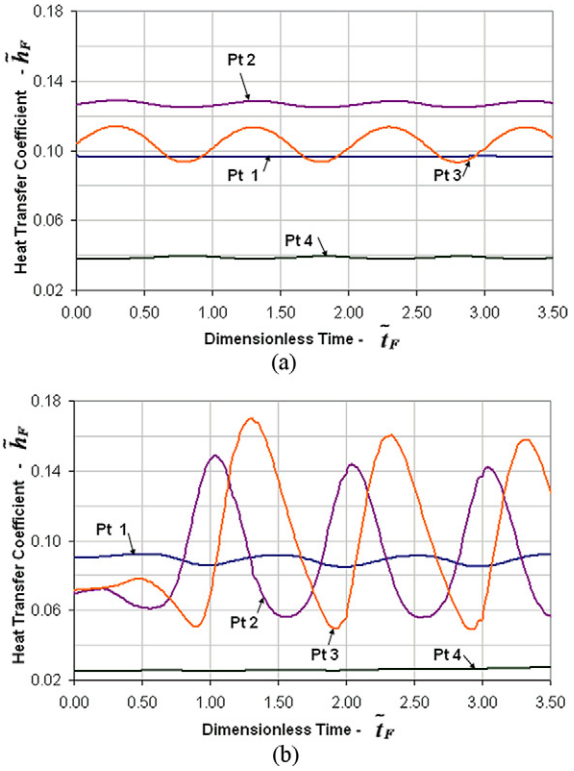

Fig. 8. Dimensionless heat transfer coefficient, $\tilde{h}_F$, results for case E arrangement with $d = 0.20$, $\omega = 2\pi$, CM/$b = 0.30$: (a) Local $\tilde{h}_F$ at four points indicated on heat source 1 in Fig. 1(a). versus dimensionless time; (b) Local $\tilde{h}_F$ at four points indicated on heat source 2 in Fig. 1(a) versus dimensionless time.

between the level of the tops of the heat sources and the bottom of the plate during the upward plate motion also frees more of the fluid passing over heat source 1 (area a in Fig. 7(a)) to enter the cavity space, moving from a to b. This fluid stream is then carried upward by the flow in the cavity and exits the cavity space to pass over heat source 2. A clockwise circulation near the left end (area f) and a counterclockwise circulation near the right end of the plate (area h) are also visible. Simultaneously, a relatively higher velocity region develops over the top of the moving plate (area g), the magnitude of which increases as the plate moves upward (Electronic Annex 5).

As the plate changes direction, the higher velocity region over the top of the plate moves to the right. At the same time, the flow area of the "opening" or cavity fluid stream (region d) entering the main natural convection induced flow in the upper channel partition is reduced, reforming the "jet-like" squeezed flow area d near the upper left corner of heat source 2 and causing a slight reduction in the net opening flow and thickening the low velocity region near the left side of heat source 2 marked by area c. As the plate continues downward, this squeezed flow becomes more x-oriented and is eventually nearly parallel to the top of heat source 2 near area e. In addition, the decreasing clearance increasingly restricts the fluid flow moving over heat source 1 from entering the cavity from under the left end of the plate near area b (Electronic Annex 5).

The values of the local heat transfer coefficients along the heat sources are good indicators of the local cooling enhancement capabilities for the configuration with the oscillating plate just over the spacing between the heat sources. Of the values at the four points on heat source 1, the heat transfer coefficient at point 3, near the right end of the top surface (near area a in Fig. 7(a)), experiences the most extensive changes over the course of an oscillation (Fig. 8(a)). The higher amplitude oscillations in the heat transfer coefficient at this location result from the periodic nature of the flows feeding the fluid streams in this area, namely the oscillatory flows induced by the plate motion and the flow moving over the top of heat source 1, above area a, which are periodically blocked from entering into the cavity region (Figs. 7, 8(a), and Electronic Annexes 5, 6). Even with the complex flow field that develops in this area marked a in Fig. 7(a), the resulting time-averaged velocities after the interaction of these flow streams are lower than at SSWONP conditions and the time averaged heat transfer coefficient is reduced by at least 5%.

The conditions at point 4 on heat source 1 show no significant improvement as well. The periodic blockage of the flow into the cavity space moving between areas a and b and the deflection of the opening flow away from the right side of heat source 1 by the presence of the plate cause lower velocities at point 4 near area b in Fig. 7(a) causing at least an 11% reduction in the local heat transfer coefficient from that at SSWONP (Electronic Annexes 5, 6, and Figs. 7, 8(a)).

At points 1 and 2, the oscillations and opening flow which are mainly transported to the right by the natural convection channel flows have little effect on the velocity and thus heat transfer rates, with between 3 and 5% decreases in the coefficient values from SSWONP (Electronic Annexes 5, 6, and Fig. 8(a)). Hence, the cooling of heat source 1 is not significantly enhanced by this arrangement.

The overall conditions at heat source 2 are generally improved by the combination method, though the cooling augmentation is largely limited to the area near the top of the heat source. Although the cross-flow is mainly directed over heat source 2 moving from area c to d to e in Fig. 7(a), the reduction in the net opening flow from that of the SSWONP configuration, caused by the obstructing presence of the plate, leads to at least an 18% drop in the heat transfer coefficient at point 1 near area c.

The diminished opening flow and the change in its path to a more rightward direction, stemming from the plate positioning and its motion, however, positively impact the heat flow from the top surface of the heat source 2. The heat flow from the top of the heat source 2 is improved because the reduced opening flow rate and the changes in the direction of the main natural convection induced flow passing near the upper left corner of heat source 2, curb the deflection of flow from the top of the heat source, near area e in Fig. 7(a) (Figs. 7, 8(b) and Electronic Annexes 5, 6). In addition, the "pulses" of higher velocity flows sweeping close to the top heat source surface described in the summary of the flow field lead to higher temperature gradients near the top surface and thus contribute to the cooling of the top surface. The local heat transfer coefficients at points 2 and 3 increase by a maximum of nearly 21% and nearly 43%, respectively (from SSWONP), with the surface average heat transfer coefficient a maximum of 28% higher. Though these coefficient values are somewhat lower than for the no plate-no opening conditions, if the trends found continue, further increases in the displacement amplitude will likely produce heat transfer coefficients that surpass those for SSNONP (Fig. 7 and Electronic Annexes 5, 6).

The higher velocity streams moving over the top of heat source 2 force the fluid away from the right side of heat source 2 causing the heat transfer coefficient at point 4 to decrease by at least 7% from SSWONP (Electronic Annexes 5, 6). The heat transfer from this surface is minimal and the impact of this reduction is not significant for the overall conditions of heat source 2 due to the low heat rates involved.

Based on the results of this investigation, the cooling enhancement with the plate oscillating atop the spacing between the heat sources is generally limited to heat source 2 and is caused mainly by the pulses of high velocity flows (generated by the plate motion and opening flow) that are carried over this heat source by the natural convection flow. Hence, while this arrangement improves the cooling of the heat source 2, any benefits on heat source 1 are minimal.

3.2.4. Oscillating plate over heat source 1—Case F

The positioning of a fixed plate just over heat source 1 as shown in case F in Fig. 1(a). significantly increased the steady state opening flow from the SSWONP conditions. The motion of the plate situated over heat source 1 with the proper clearance and oscillation parameters can sustain the increased opening flow that is used to essentially augment the cooling of the second heat source, while positively impacting the cooling

of heat source 1. Adequate oscillation induced cooling of the heat source 1 with minimal blockage of the flow over either heat source was made possible by the selection of a relatively large mean clearance spacing. Increases in the displacement amplitude enhance the oscillation related cooling effect at heat source 1 with the plate motion holding little influence over the thermal conditions at heat source 2. The major results for this arrangement are summarized in Table 3. See Electronic Annex 7 in the online version of this article for the velocity distribution for the case with $d = 0.20$, $\omega = 4\pi$ and Electronic Annex 8 for an animation of the corresponding temperature distribution as well as Fig. 9. The local heat transfer coefficients for this parameter set are shown in Fig. 10.

The following general description of the common velocity field characteristics for the case F arrangement is intended to facilitate an understanding of the means and locations of improved thermal conditions. As the downward moving plate comes to a stop at its lowest position, the outgoing flow from either end of the plate together with the other flow-drivers cause a clockwise (CW) circulation to the left side and slightly above the moving plate (area a in Fig. 9(a)), and a counter-clockwise (CCW) circulation region just to the right of the plate (area c in Fig. 9(a)) (Electronic Annexes 7, 8). These circulations restrict the potential fluid flow paths around the heat sources. A fluid stream moving over the top of the left CW circulation (a) and over the top of the plate and heat source 1 is directed downward by this left circulation and is carried under the right circulation near area c towards the fluid stream just above the label d in the Fig. 9(a). The portions of the flows moving near the circulation c and the stream above the d label which move over the cavity between the heat sources are diverted away from heat source 2 by the upward moving CCW circulatory flow of the circulation around area c and the opening flow moving out of the cavity space between the heat sources near area f in Fig. 9(a) (Electronic Annex 7). Within the cavity space, the majority of the opening cross-flow proceeds to the right towards area f, away from area e, and is then carried with flow stream h over heat source 2.

As the plate moves upward, the clearance under the plate, area b in Fig. 9(a), widens and is filled with fluid entering through both plate ends. The left CW circulation, area a, is pushed to the right over the top of the plate by the rightward moving natural convection and plate motion induced flows. This relocation, which shortens the distance between the circulations, increases the velocities of the fluid forced under the right CCW circulation, area c, and, hence, the velocities near

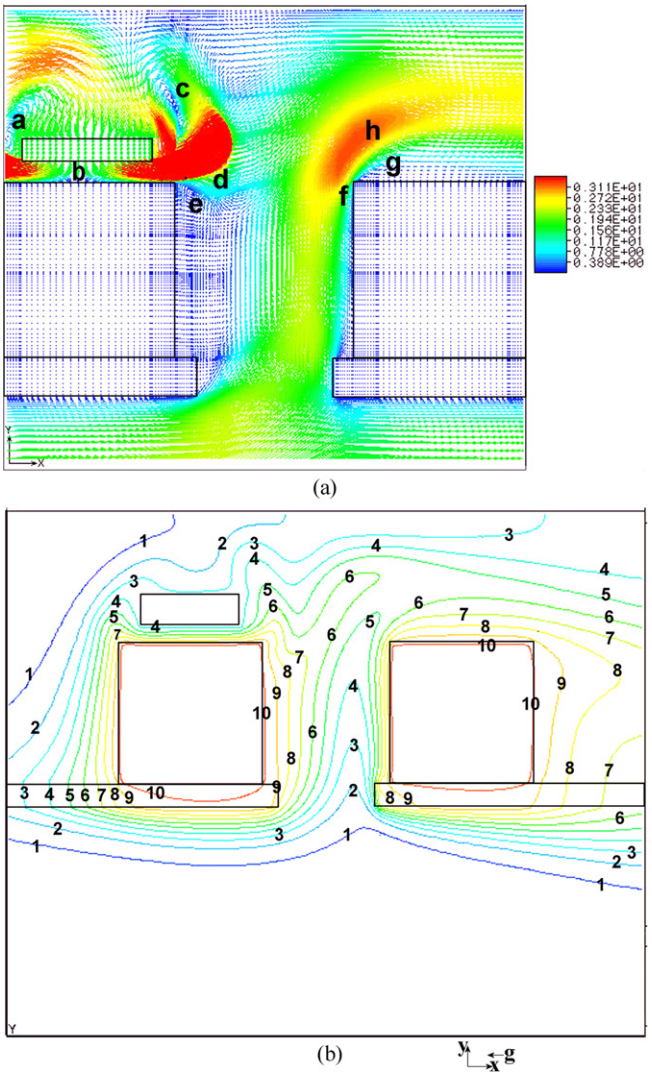

Fig. 9. Sample results near heat sources for case F arrangement with $d = 0.20$, $\omega = 4\pi$, CM/$b = 0.30$ at $\tilde{t}_F = 0.820$: (a) vector plot of dimensionless velocity field $[\tilde{u}_F, \tilde{v}_F]$; (b) Contours dimensionless temperature, $\widetilde{T}_F$: Value of temperature of contour labeled M is 0.0875[2M-1].

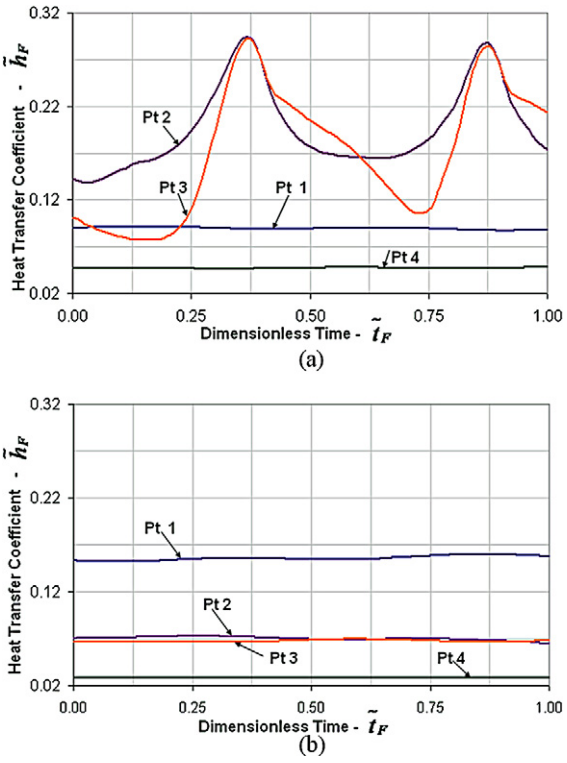

Fig. 10. Dimensionless heat transfer coefficient results, $\tilde{h}_F$, for case F arrangement with $d = 0.20$, $\omega = 4\pi$, CM/$b = 0.30$: (a) Local $\tilde{h}_F$ at four points indicated on heat source 1 in Fig. 1(a) versus dimensionless time; (b) Local $\tilde{h}_F$ at four points indicated on heat source 2 in Fig. 1(a) versus dimensionless time.

the upper right corner of the heat source 1, near area d. The flow brought to this corner area then forms two branches. One branch carries the flow to the right with the natural convection induced upper channel flow and enters the cavity between the heat sources passing near area e. The second branch carries the fluid to the left and under the plate to area b (Electronic Annex 7). As time progresses, the flows transporting fluid into the clearance become strong enough to dissipate the original circulations, and then to help form new oppositely directed circulations at the ends of the plate. These circulations do eventually move under the oscillating plate. The combined effects of the increased flow drawn into the clearance and the increased flow around the circulation at the right end of the plate, area c, pull a small segment of the opening flow in the cavity towards areas d and e and the right end of the plate and heat source 1. The majority of the opening flow continues to move over heat source 2 from area f to h to g, thinning the low velocity regions near the left and top surfaces of heat source 2 particularly near area f.

As the plate reaches its maximum position, the larger clearance space facilitates through-flow under the entire plate length (through area b) that proceeds around the existing circulations that are typically within the clearance. The interaction of clearance through-flow, the opening flow being drawn to areas d and e, the circulations, and the flow moving off of the top of the plate forms a low velocity region just to the right of the plate and heat source 1. This, in turn, changes the magnitude and direction of the main channel flows passing near the top of heat source 2. The altered flow pattern reduces the diversion of flow from the top surface of heat source 2 near area g and helps increase the heat removal from this heat source 2 surface (Electronic Annex 7).

The plate then turns downward. The fluid inertia effects encourage the maintenance of the through flow stream that proceeds under the left circulation, a, and over the right circulation, c, both of which have moved slightly under the plate. Despite the downward motion of the plate, some fluid even enters from under the right circulation to help cool the region d area. The increase in the plate velocity and the decrease in the clearance eventually forces fluid to move out of both ends of the clearance space (Fig. 9). These flows dissipate the circulations, which is particularly important in altering the angle at which the fluid exits and enters the right end of the clearance near area d in Fig. 9(a). As these higher, more x-oriented, velocity flows moving directly to the right of the plate meet with the opening flow, the deflection of the flow from the top of heat source 2 near area g in Fig. 9(a) (Electronic Annex 7) is increased. Also, the remnants of the right circulation cause a fluid stream to dip into the cavity space near area e. This results in an increase in the cooling of the right side of heat source 1 near area e in Fig. 9(a).

As the plate motion induced flows become stronger as the plate continues to move downward, circulations re-form to the sides of the plate at areas a and c in Fig. 9(a) (CW left and CCW right) and the low velocity region left by the previous circulation zone moves away. A more intense flow exiting through the right end of the clearance, near the area marked d, runs almost parallel to the plate and the fluid no longer dips into the cavity space. These effects further redirect the path of the opening flow near area f that enters the upper channel, and causes noticeably thicker lower velocity areas near the left and top sides of heat source 2 near area f and g (Fig. 9 and Electronic Annex 7). However, no significant blockage of the net opening flow develops. The cycle then repeats.

The minimal obstruction of the opening flow over the course of a plate oscillation for this configuration is confirmed upon examination of the cross-flow rate results. While there is net flow into the upper channel, comprising, at maximum, 54% of the flow exiting the upper channel at SSWONP during one plate oscillation, the instantaneous variation in the flow is only about 1%. Thus, the cross-flow is sustained and is able to significantly contribute to the cooling of especially heat source 2.

The cooling effect for this arrangement is briefly described in terms of the impact that the velocity field characteristics described above have on the resulting heat transfer coefficients at the heat sources. The general diversion of flow from the left side surface of heat source 1 resulting from the higher speed flows exiting and entering the clearance leads to at least an 11% reduction in the heat transfer coefficient at point 1 relative to SSWONP with little change over an oscillation (Electronic Annexes 7, 8, and Fig. 10(a)).

The movement of fluid from over the top of the plate and from within the clearance space into the cavity near area e in Fig. 9(a) as well as the movement of some opening flow towards the right side of this heat source during portions of the cycle create higher overall velocities near the right side, bringing about as much as a 10% increase in the local heat transfer coefficient at point 4 compared to SSWONP (21% in the surface average) although there is little variation over a cycle.

The most impressive cooling occurs at points 2 and 3 (on the top surface due to the high velocity streams like region d in Fig. 9(a)), where the local heat transfer coefficients are as much as 49% and 70% higher than those for SSWONP respectively, and 40% and 50% higher than those for SSNONP (Electronic Annexes 7, 8, and Fig. 10(a)). The top surface average heat transfer coefficient is as much as 47% greater than that at SSWONP and 37% greater than SSNONP. Since the opening flow is directed mainly to the right of the opening away from area e in Fig. 9(a), these results indicate that the oscillations are mainly responsible for the significant improvement in the overall thermal conditions of heat source 1.

At heat source 2, the results suggest that the system geometry with the plate in this configuration, not the motion of the plate, holds more influence on the thermal conditions of this heat source. This is apparent in the slight variation in the heat transfer coefficients at heat source 2 with time in Fig. 10(b). The placement of the plate over heat source 1 increases the cross-flow rate as explained in the steady state results earlier. In addition to the higher velocities and greater opening flow rates, this generally allows the cross-flow to more closely follow particularly the left side of heat source 2 near area f in Fig. 9(a) compared to a system with no plate. Hence, at heat source 2, the left side receives the most benefit from the flow fields that develop as the local heat transfer coefficient at point 1 increases by a maximum of 44% from that at SSWONP (441% higher than SSNONP) (Electronic Annexes 7, 8, and Figs. 9, 10(b)).

The surface average heat transfer coefficient at the left side increases by 37% from SSWONP and 193% from SSNONP.

However, the increased opening flow heightens the diversion of flow from the top surface near area g in Fig. 9(a) of the heat source with the local heat transfer coefficients at points 2 and 3 at best between 6% and 10% lower than SSWONP respectively and 40% to 50% lower than SSNONP. The top surface average heat transfer coefficient is at a minimum 7% lower than that at SSWONP and at least 40% lower than for SSNONP (Electronic Annex 7, 8, and Figs. 9, 10(b)).

The plate configuration, the opening flow and the oscillations have little effect on the right side surface of heat source 2 compared to SSWONP at point 4 (Electronic Annexes 7, 8, and Fig. 10(b)).

The results show that the higher heat transfer from the left side surface of heat source 2 caused by the stronger opening flow substantially improves the overall thermal conditions at this heat source despite the negative effects at the top of the heat source. The average temperature of heat source 2 in a system with an opening and with the fixed plate is about 27% lower than that for a no opening and no plate system and 12% lower than that with only the opening.

Among the configurations investigated, the case F geometry produces the lowest overall operating temperatures and the highest overall heat transfer coefficients over both heat sources relative to the opening-no plate geometry. The oscillations are responsible for the majority of the cooling of heat source 1 while the higher opening flow is responsible for the majority of the improvement in the thermal conditions of heat source 2. As a result, for the parameters studied, this is the most beneficial arrangement investigated.

4. Conclusions

The enhancement of natural convection in a vertical channel by the oscillations of a discrete plate combined with the cross-flow through a board opening was investigated in parametric finite element studies. The following summarizes the important conclusions:

(1) The combined use of a strategically positioned oscillating plate and a strategically placed cross-flow opening can significantly improve the local cooling of heat sources in comparison to pure natural convection.
(2) The cooling enhancement produced by this method is of a focused, targeted, and localized nature, which is difficult to achieve with commonly used techniques, such as the rotating fan.
(3) The cooling effect generated by this method is most influenced by the positioning of the plate relative to the heat sources and the opening for a given heat source array. Among the geometries investigated for the two heat source array studied, the arrangement with the vibrating plate placed over the heat source to the left or upstream of the opening, case F, provided a superior performance for improving the overall thermal conditions of both heat sources. The oscillations worked to cool mainly the left heat source with as much as a 70% rise in the local heat transfer coefficient with respect to a system with no plate but with the opening or a 55% improvement over that with no plate and no opening. The cross-flow through the opening is chiefly responsible for the enhanced cooling of the right heat source with up to a 44% improvement in the local side surface heat transfer coefficient relative to that for a system with the opening, but no plate or over a 440% rise from that with no plate and no opening.
(4) The oscillations were shown to be most beneficial when generated in the immediate vicinity of the heat source, while the opening cross-flow is most advantageous when the obstruction of the flow paths near, and especially to the right or downstream, of the opening is minimized.
(5) For the arrangements and parameters investigated, the cooling level attained was more dependent on the plate displacement than on its frequency. For some cases, increasing the plate frequency, while holding the displacement fixed, lead to a diminished cooling effect.
(6) A properly designed cooling system utilizing this combined method can thus serve as a viable alternative to provide localized cooling of low power devices that cannot be properly cooled by pure natural convection, before the use of the conventional rotating fan with its disadvantages is needed.

Based on the results of this study, further investigation of this technique including experimental verification and applications to a larger array of heat sources is warranted.

Supplementary material

Supplementary data associated with this article can be found, in the online version, at doi:10.1016/j.ijthermalsci.2006.03.007.

References

[1] S.K.W. Tou, C.P. Tso, X. Zhang, 3-d numerical analysis of natural convective liquid cooling of a 3 × 3 heater array in rectangular enclosures, International Journal of Heat and Mass Transfer 42 (1999) 3231–3244.
[2] L.T. Yeh, Review of heat transfer technologies in electronic equipment, J. Electron. Packag. 117 (1995) 333–337.
[3] V.H. Adams, Y. Joshi, D.L. Blackburn, Three-dimensional study of combined conduction, radiation, and natural convection from discrete heat sources in a horizontal narrow-aspect-ratio enclosure, J. Heat Transfer 121 (1999) 992–1001.
[4] F.P. Incropera, Future research directions, in: W. Aung (Ed.), Cooling Technology For Electronic Equipment, Hemisphere, New York, 1988, pp. 800–821.
[5] F.P. Incropera, Liquid Cooling of Electronic Devices, Wiley, New York, 1999, pp. 1–14.
[6] R.E. Simons, The evolution of IBM high performance cooling technology, IEEE Trans. Components, Packaging, and Manufacturing Technology Part A 118 (1995) 805–811.
[7] T.C. Hung, C.S. Fu, Conjugate heat transfer analysis for the passive enhancement of electronic cooling through geometric modification in a mixed convection domain, Numer. Heat Transfer Int. J. Comput. Methodol. Part A Appl. 35 (1999) 519–535.
[8] S. Sathe, A review of recent developments in some practical aspects of air-cooled electronic packages, J. Heat Transfer 120 (1998) 830–838.
[9] R. Viswanath, Thermal performance challenges from silicon to systems, Intel Journal Q3, www.intel.com (2000) retrieved November 23, 2000.

[10] J.H. Yoo, J.I. Hong, C.Y. Park, Characteristics of piezoelectric fans using pzt ceramics, Paper presented at the 5th International Conference on Properties and Applications of Dielectric Materials, Seoul, South Korea, 1997.
[11] J.H. Yoo, J.I. Hong, W. Cao, Piezoelectric ceramic bimorph coupled to thin metal plate as cooling fan for electronic devices, Sens. Actuators A Phys. 79 (2000) 8–12.
[12] R.R. Schmidt, Local and average transfer coefficients on a vertical surface due to convection from a piezoelectric fan, Paper presented at the InterSociety Conference on Thermal Phenomena, 1994.
[13] A. Kruusing, et al., Heat Transfer Enhancement at solid–liquid and solid–gas interfaces by near surface cooling agitation, IEEE Trans. Components and Packaging Technologies 23 (2000) 548–554.
[14] T. Acikalin, S.M. Wait, S.V. Garimella, A. Raman, Experimental investigation of the thermal performance of piezoelectric fans, Heat Transfer Engineering 25 (2004) 4–14.
[15] P. Burman, A. Raman, S. Garimella, Dynamics and topology optimization of piezoelectric fans, IEEE Trans. Components and Packaging Technologies 24 (2003) 592–600.
[16] S.H. Kim, N.K. Anand, Use of slots to enhance forced convective cooling between channels with surface-mounted heat sources, Numer. Heat Transfer Int. J. Comput. Methodol. Part A Appl. 38 (2000) 1–21.
[17] T.C. Hung, S.K. Wang, F.P. Tsai, Simulations of passively enhanced conjugate heat transfer across an array of volumetric heat sources, Comm. in Numerical Methods Engrg. 13 (1997) 855–866.
[18] T.C. Hung, A conceptual design of thermal modeling for efficiently cooling an array of heated devices under low Reynolds numbers, Numer. Heat Transfer Int. J. Comput. Methodol. Part A Appl. 39 (2001) 361–382.
[19] L.A. Florio, Static and dynamic methods of enhancing pure natural convection cooling of electronics, PhD thesis, New Jersey Institute of Technology, Newark, New Jersey, 2005.
[20] L.A. Florio, A. Harnoy, Feasibility study of unconventional cooling of electronic components by vibrating plates at close proximity, Numer. Heat Transfer Int. J. Comput. Methodol. Part A Appl. 47 (2005) 997–1024.
[21] A.-R.A. Khaled, K. Vafai, Nonisothermal characterization of thin film oscillating bearings, Numer. Heat Transfer Int. J. Comput. Methodol. Part A Appl. 41 (2002) 451–467.
[22] A.-R.A. Khaled, K. Vafai, Analysis of flow and heat transfer inside oscillatory squeezed thin films subject to a varying clearance, International Journal of Heat and Mass Transfer 46 (2003) 631–641.
[23] D.J. Radakovic, M.M. Khonsari, Heat transfer in a thin film flow in the presence of a squeeze and shear thinning: application to piston rings, J. Heat Transfer 119 (1997) 249–257.
[24] F. Bade, P. Haldenwang, Higher order scheme for thermally driven flows in an open channel, Computers and Fluids 27 (1998) 273–290.
[25] FIDAP user's manual. Retrieved August 15, 2001 from: http://www.cae.wisc.edu/manuals/fluent5.2/fidap.